Development of nonlinearity in a growing self-excited dust-density wave

T. M. Flanagan and J. Goree
Department of Physics and Astronomy, The University of Iowa, Iowa City, Iowa 52242, USA

(Received 18 November 2010; accepted 2 January 2011; published online 26 January 2011)

The development of nonlinearity is observed in a naturally occurring planar dust-density wave. As it propagates through a dusty plasma, the wave grows and harmonics are generated. The amplitudes, wave numbers, and growth rates are measured for the fundamental and its harmonics. The energy in the harmonic modes exhibits a strong exponential increase with diminishing gas pressure, until it levels off at lower gas pressures. The wave numbers and growth rates for the harmonics are near integer multiples of those for the fundamental. © *2011 American Institute of Physics*.
[doi:10.1063/1.3544938]

I. INTRODUCTION

Dust-acoustic waves, also termed dust-density waves, are low-frequency compressional waves that propagate in dusty plasma.[1] (Dusty plasma is a collection of small charged dust particles in a plasma background of electrons, ions, and neutral gas.) The dust-density wave (DDW) is analogous to the ion-acoustic wave. In the DDW, the heavy dust particles provide the wave's inertia. During compression and rarefraction of the dust particles, charge separation from the background electrons and ions contributes to a restoring electric field. The electric forces can be large because the dust particles have a large negative charge. Because the dust particles are so heavy, the DDW frequency is very low. Thus, the wave can be observed in the laboratory using video imaging.[2]

A DDW is often self-excited naturally in dusty plasma due to an instability driven by ion flow.[3,4] This has been observed in several experiments, both in the laboratory[5–14] and under microgravity conditions.[15,16] In laboratory experiments dust particles are often levitated in the plasma sheath, where ion flows can be strong enough to couple their energy to dust particles and drive the wave.[3]

The DDW can be driven to large amplitudes, where a variety of nonlinear effects have been observed. Shocks have been shown to develop as a DDW steepens,[17,18] and a confluence of shocks has been observed.[19] Nonlinear wave-particle interaction[12,20,21] and wave breaking[24] have been observed in experiments that allow identification of individual particles. Turbulence,[22] spatial frequency clustering,[23] and wave harmonics[20,24] have also been reported. These experiments were mostly performed under conditions where dissipation could not stop the wave from growing to large amplitudes.

The DDW is damped by collisions between dust particles and neutral gas, which is always present in dusty plasma experiments. At high gas pressures, the dust-neutral collision rate ν_{dn} is so large that the wave is not observed, while at low gas pressures, gas damping is less effective and the DDW can grow to large amplitudes.[4] At a critical gas pressure, the instability and gas damping balance, which determines a threshold for wave excitation.[4,9,12,25,26] At gas pressures of about 1 Torr (1 atm=760 Torr), the time scale for gas damping of dust motion ν_{dn}^{-1} is comparable to a typical wave period. For a spherical dust particle of radius r_d and mass density ρ_d, the dust-neutral collision rate is $\nu_{\mathrm{dn}}=\sqrt{8k_BT_gm_g}\delta n_g/\rho_d r_d$, where m_g is the mass of a gas atom, T_g and n_g are the gas temperature and number density, and δ is a constant of order unity that must be measured.[27] Because ν_{dn} is proportional to n_g, it is also proportional to gas pressure. In the experiment reported here, we reduce the effect of gas damping by decreasing the gas pressure.

While most experimenters agree that dust-neutral collisions are responsible for DDW damping under typical laboratory conditions, other damping mechanisms have also been proposed. One of these is wave damping due to a fluctuating dust particle charge.[28–30]

Here, we report the observations of the development of nonlinearity in a coherent self-excited DDW. As we gradually reduce gas pressure p (i.e., gas damping), we at first observe a small amplitude wave. As we reduce p further the wave amplitude increases and nonlinearity develops. We quantify nonlinearity by detecting harmonics. We measure the amplitude, wave number, and growth rate of each harmonic using a phase-sensitive detection.[26] We find three conditions: at high gas pressures p the harmonics cannot be distinguished from noise; at intermediate p the harmonic energies emerge from the noise and increase exponentially as p decreases; and finally at lower p the harmonic energies level off. We find that the values of the wave numbers k_r and growth rates k_i for the second harmonic (frequency $2f$) are double those for the fundamental (frequency f). Similarly, k_r and k_i for the third harmonic ($3f$) are triple those for the fundamental.

II. EXPERIMENTAL DESIGN

The experiment is designed to observe the development of nonlinearity in a naturally occurring dust-density wave. To do so, we begin the experiment under conditions where the dusty plasma exhibits little or no wave activity. We then use the gas pressure as a control parameter for the ion-flow instability. We use a design with an electrode and a glass box that confines a dust cloud with a symmetry that helps simplify the analysis of wave propagation.[26]

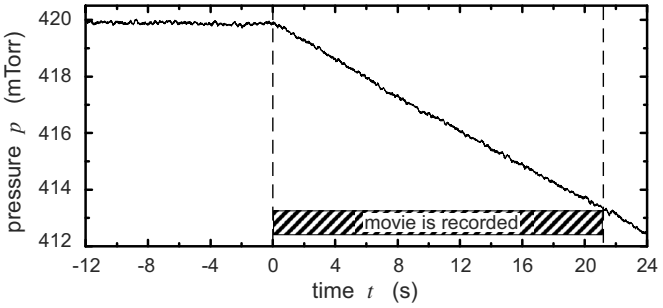

FIG. 1. Time series measurement of gas pressure p, which is the experimental parameter used to control the instability and growth of the dust-density wave. The pressure is constant until time $t=0$ when we begin to decrease pressure at a linear rate. At the same time, we begin recording a movie, which provides our principal data.

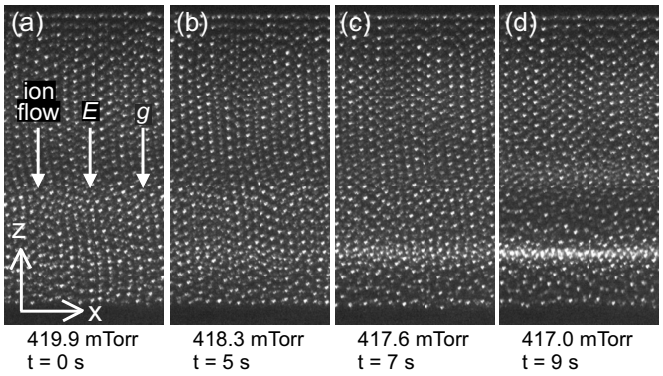

FIG. 2. Side view images of the dust cloud's central region. Bright spots are individual dust particles. At lower gas pressures, the ion-flow instability can cause planar compressional waves to grow in amplitude as they propagate downward in the $-\hat{z}$ direction. (a) At the highest pressure, gas damping causes the wave to be barely detectable. [(b)–(d)] At lower gas pressures, gas damping is less effective and the wave grows to higher amplitudes, as indicated by the bright high-density wave fronts near the bottom of the dust cloud. Each panel shows the same 2.95 mm × 5.90 mm spatial region. The online reader may view a portion of the movie showing both the wave's growth as it propagates downward and the amplitude increase as pressure diminishes. The movie clip, which plays at reduced speed, corresponds to the time interval between $t=4$ and $t=12$ s (enhanced online). [URL: http://dx.doi.org/10.1063/1.3544938.1]

A. Dust cloud confinement and imaging

A quantity of about 10^5 dust particles (4.8 μm diameter) are introduced into an argon plasma. The dust particles become negatively charged and are levitated in the plasma sheath's vertical electric field. They fill a volume in the plasma near the bottom of a glass box.[26] The box, which rests on a rf powered electrode, has vertical walls, so that the plasma develops a significant horizontal electric field. The combination of vertical and horizontal electric fields confines dust particles in a cloud. The dust cloud has a 22 mm width, and it has many horizontal layers so that it has a 6 mm height. The dust cloud is viewed from the side using a high-speed camera that records a 21 s movie at 500 frames/s.

We verified that the camera has a linear response and the dust cloud is optically thin. Therefore, the scattered light and the image intensity are proportional to dust number density.[26]

The confining electric fields for our electrode and glass box design help provide nearly one-dimensional waves. Ions flow vertically downward, and there is little vertical or horizontal variation in dust number density. As a result of this symmetry, we will find that waves propagate downward, parallel to ion flow, with nearly planar horizontal wave fronts. The planarity of the wave fronts allows straightforward measurements of one-dimensional wave propagation and growth. Because the ion flow causes the wave to grow as it propagates, nonlinear effects are expected to be small at the top of the dust cloud and increase downward. This spatial growth of amplitudes allows us to observe the development of nonlinearities.

B. Pressure control

The DDW amplitudes, and therefore the expected nonlinear effects, vary sensitively with gas pressure p, which leads us to design an experiment where we vary p over many finely spaced values. Therefore, we choose to sample data as we vary the gas pressure slowly and gradually (see Fig. 1), rather than record data at discrete pressure levels, as we did previously.[26]

The experiment begins with a dust cloud at $p=420$ mTorr, which is just below the critical gas pressure so that wave activity is barely detectable. At this pressure, the gas damping rate is $\nu_{dn}=135\ s^{-1}$. A side view image of the dust cloud under these conditions is shown in Fig. 2(a). We note that, in this stable dust cloud, the dust particles tend to line up in vertical chains. This vertical alignment is due to the downward ion flow,[31] which is the same flow that can excite the DDW.

We use a pressure control system to decrease the gas pressure continuously, Fig. 1. The control system consists of a capacitance manometer pressure sensor, a butterfly exhaust valve to regulate the pumping speed, and a feedback controller that adjusts the valve in order to match the pressure measurement to a desired set point. In order to ramp the pressure linearly with time, we apply a corresponding voltage waveform to the controller's set point. Only the pumping speed is adjusted in this control system; the inlet gas flow remains constant at 5 SCCM (SCCM denotes cubic centimeter per minute at STP).

The requirement that must be met, in choosing the pressure ramp rate, is to observe multiple wave transits under nearly steady conditions. (A wave transit in our experiment requires 0.15 s; this is the time required for the DDW to propagate through the dust cloud's vertical extent.) The most restrictive conditions for meeting this requirement are found in the intermediate pressure range, where wave amplitude is most sensitive to pressure. We will find that in the intermediate pressure range, harmonic energies will increase by a factor e over a pressure change of 0.24 mTorr. We choose a ramp rate to be slow enough that there are multiple wave transits during the time interval that the pressure changes by 0.24 mTorr. We used a ramp rate of -0.31 mTorr/s, corresponding to a 0.01% decrease of pressure and damping rate during one wave transit. The duration of our entire movie, 21 s, corresponds to 140 wave transits.

III. WAVE AMPLITUDE OBSERVATIONS

Our results are all based on the movie, which reveals a coherent self-excited dust-density wave. The wave has a nearly planar geometry. The properties and development of the wave are easily seen in the recorded movie, Fig. 2. The wave propagates downward through the dust cloud in the $-\hat{z}$ direction, parallel to the ion flow. The phase speed of 40 mm/s and frequency of 25.0 Hz did not vary significantly over the entire vertical height of the dust cloud.

Nonlinear effects are expected where wave amplitudes are highest, which we observe in this experiment near the bottom of the dust cloud and at lower gas pressures. Near the bottom of the cloud, the amplitude is large because the wave grows as it propagates downward. This spatial growth is due to the ion-flow instability, which drives the wave. The spatial growth is prominently indicated by the increasing amplitude of the wave fronts near the bottom of the dust cloud in Fig. 2(d), as compared to the top. At lower gas pressures, the amplitude is large because gas friction is reduced. Gas friction is an energy loss mechanism that competes with the instability.[4,26] The variation of wave amplitude with gas pressure can be seen by comparing the four panels of Fig. 2, and by noting that for a given height z, the wave amplitude increases as the pressure is lowered.

IV. ANALYSIS METHODS

The three main methods used to analyze our recorded movie are calculations of space-time data, power spectra, and a phase-sensitive amplitude detection. These are all based on analyzing video images, where the brightness of the image is proportional to dust number density. Details of these three methods are presented next.

The first method is a calculation of space-time data, which represent image intensity as functions of both vertical position z and time t. The calculation begins with individual video images, cropped to the spatial region shown in the panels of Fig. 2 (5.90 mm vertical and 2.95 mm horizontal). Exploiting the planar nature of the waves in this region, we average over an ignorable coordinate x, yielding data corresponding to dust number density versus vertical position z. All the required information needed to analyze a compressional planar wave is incorporated into the space-time data: a quantity representing dust number density as a function of both position z and time t. Details of the calculation method are described in our previous paper,[26] where space-time data (for a different experiment) are presented in a visual form as a space-time diagram.

The second method is an identification of the frequencies present in the wave using power spectra computed as functions of vertical position z. For a given height z, a power spectrum is computed from the space-time data using an fast Fourier transform (FFT) of a 1024 frame ($\sim$2 s) time series. This is repeated for 30 vertical positions z. Assembling the power spectra for each value of z yields a plot of wave energy as a function of both frequency and height. These spatially resolved plots of the power spectrum will reveal a fundamental frequency as well as the presence of harmonics.

The third method is a phase-sensitive amplitude detection,[26] which yields precise measures of the phase ϕ and amplitude A as functions of the vertical position z. For a given height z, the phase and amplitude are detected using a short time series from the space-time data. The detection of phase and amplitude is based on principles analogous to those of an electronic instrument called a lock-in-amplifier.[32] Like a lock-in-amplifier, our detection requires a reference wave at a known frequency, which we synthesize using the frequency measured from the power spectra. We repeat the calculations of $\phi(z)$ and $A(z)$ separately for the fundamental frequency f and the harmonics $2f$ and $3f$. This method requires that the frequency does not vary with position z, and that it varies slowly or not at all with time. These requirements are satisfied in our experiment. Phase-sensitive detection allows us to analyze shorter time series of data (0.2 s). In this experiment, time has a direct correspondence with gas pressure. Further details of phase-sensitive detection are provided in a previous paper.[26]

Our chief results, in Sec. V, are based on measurements of amplitude A and phase ϕ using the phase-sensitive detection. One of our chief results will be a characterization of the pressure dependence of nonlinearity, which we quantify using the total harmonic distortion computed from amplitudes of the harmonics and fundamental. Another chief result is the measurement of wave number k_r, and growth rate $-k_i$, using a method we describe next.

We measure k_r and $-k_i$ separately for the fundamental and each harmonic using the spatial profiles of phase $\phi(z)$ and amplitude $A(z)$. We assume planar waves with a dust number density $\propto e^{ikz-i2\pi ft}$, where the real part of $k=k_r+ik_i$ is the wave number and the imaginary part corresponds to the growth rate. We find k_r as the slope of $\phi(z)$. We find the growth rate $-k_i$ by fitting $A(z)$ to an exponential; this pure exponential variation requires planar wave fronts. We measure $-k_i$ only in the upper and middle spatial regions, where the wave amplitude grows as $e^{-k_i z}$ and is not yet saturated.

V. RESULTS

A. Fundamental frequency

The fundamental frequency of the wave is $f=25.0$ Hz. This measurement is based on the power spectrum, Fig. 3. For our experimental design, we found that f did not vary significantly with vertical position z or gas pressure p.

B. Development of nonlinearity with diminishing pressure

We will present several results to study the development of a nonlinear wave as gas pressure p decreases. We begin by observing the presence of harmonics in the power spectrum. We will then use phase-sensitive detection to quantify how the harmonics emerge, grow, and then level off as the gas pressure is diminished.

The presence of harmonics is a signature of nonlinearity, and is revealed in the power spectra (Fig. 3). The energy in the harmonics exhibits the same general trends as the energy of the fundamental: all become stronger at lower gas pres-

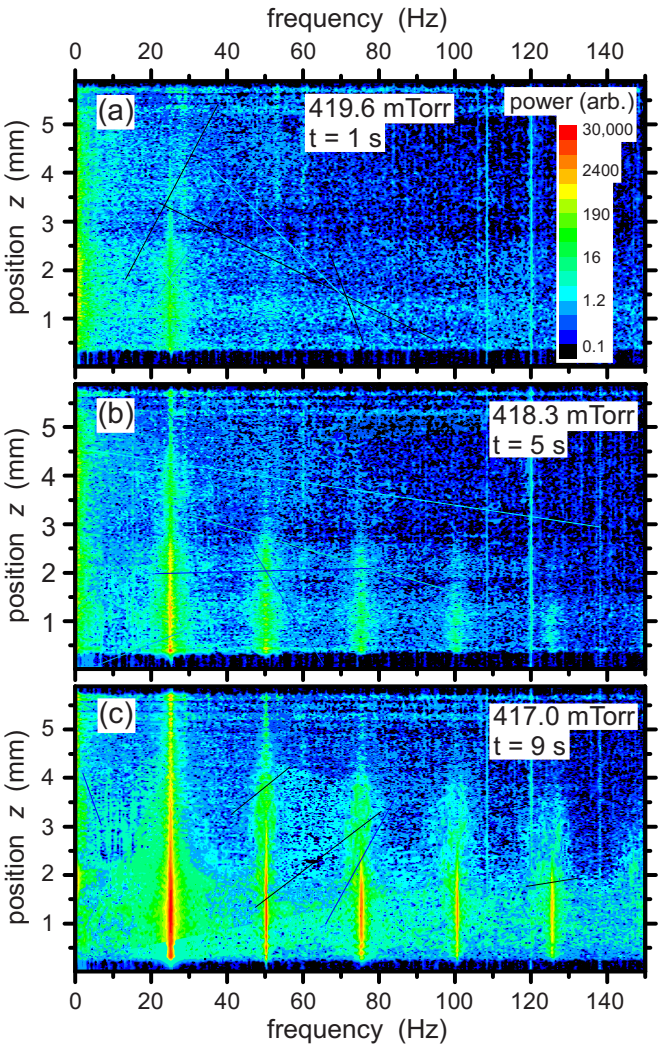

FIG. 3. (Color online) Power spectra plotted vs vertical position z for three gas pressures. The fundamental frequency is f=25.0 Hz. (a) At high gas pressures, we can detect only the fundamental and only at lower values of z. [(b)–(c)] At lower pressures, harmonics become stronger. At 417 mTorr, we can detect all nine harmonics that are below the Nyquist frequency; only the first four are shown. These spectra are calculated from the space-time data; each panel corresponds to a sequence of 1024 frames, i.e., 2 s of data, centered at the times indicated. (The zero for vertical position z is arbitrarily chosen to be just below the bottom of the dust cloud.)

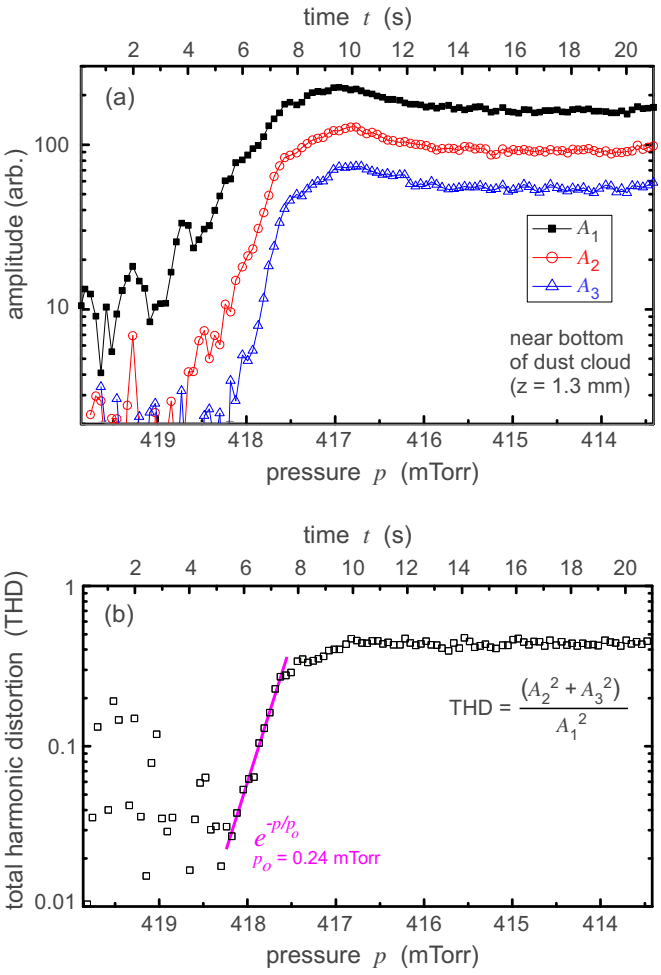

FIG. 4. (Color online) Results showing the pressure dependence of the fundamental and harmonics for a position near the bottom of the dust cloud. (a) Amplitudes of the fundamental A_1, the second harmonic A_2, and the third harmonic A_3. As pressure p decreases, all amplitudes increase exponentially from the noise and then level off. (b) THD, an indicator of nonlinearity, calculated from the amplitudes in (a). After emerging from the noise, the THD increases exponentially as p decreases, with a pressure constant p_o, and then levels off at 45%; i.e., the harmonic energy at lower pressures is almost half the fundamental energy. Noise on the left is due to small wave amplitudes. In both panels, the gas pressure scale is reversed (bottom axis). Results here and in Fig. 6 are computed from the space-time data using phase-sensitive detection.

sures and near the bottom of the dust cloud, i.e., at small z. At higher pressures, the wave amplitude is very small so that only the fundamental is detectable, especially near the bottom of the dust cloud, as in Fig. 3(a).

The growth of the fundamental and harmonics is measured with a better precision and resolution by the phase-sensitive detection. For a position near the bottom of the dust cloud, Fig. 4(a), we see that the fundamental amplitude A_1 increases exponentially with decreasing pressure, after emerging from noise. This exponential increase is abrupt, with the amplitude doubling several times as the pressure is reduced only a fraction of 1%. As p decreases further, the exponential variation ceases and the amplitude levels off. The harmonics exhibit the same trends as pressure decreases: emerging from noise, then increasing exponentially, and finally leveling off at lower pressures. However, compared to the fundamental, the harmonics emerge from noise at slightly lower pressures, and they level off at lower amplitudes.

As a simple indicator of nonlinearity, we use the total harmonic distortion (THD), which is the ratio of the total energy in the harmonics to the energy in the fundamental. In Fig. 4(b), we calculate the THD as $(A_2{}^2+A_3{}^2)/A_1{}^2$, using the amplitudes from Fig. 4(a).

We find three conditions in the development of nonlinearities, as measured by THD. First, nonlinearity emerges from the noise level at a pressure of about p=418.2 mTorr. Second, the nonlinearity increases exponentially as p is reduced, $\propto e^{-p/p_o}$. Fitting the data in Fig. 4(b) we find a small value for the fit constant of p_o=0.24 mTorr. The exponential increase of nonlinearity does not continue indefinitely as p decreases. In fact, it occurs only over a limited range of pressures. Third, the THD levels off at about 45%. In other

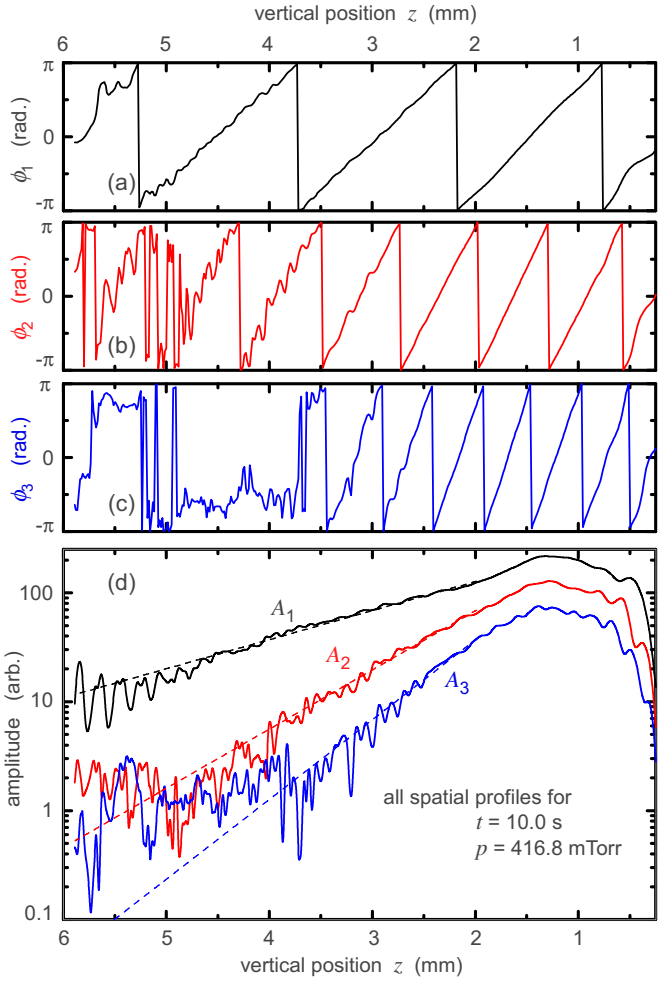

FIG. 5. (Color online) Vertical profiles of [(a)–(c)] the wave's phase ϕ and (d) the wave's amplitude A, corresponding to gas pressure p =416.8 mTorr. Results are shown for the fundamental wave mode (ϕ_1, A_1) and its second and third harmonics, (ϕ_2, A_2) and (ϕ_3, A_3). Profiles like these are calculated from space-time data using phase-sensitive detection. These profiles are then used to measure the wave numbers k_r and growth rates $-k_i$.

words, the nonlinearity increases to a maximum level where energy in the harmonics is almost half the energy in the fundamental. This 45% THD was measured for a position z =1.3 mm near the bottom of the dust cloud. At higher positions, the nonlinearities are weaker, with a THD of 40% at z=2.0 mm and 10% at z=3.0 mm.

C. Phase and amplitude profiles

Our phase-sensitive detection yields vertical profiles of the phase ϕ and the amplitude A for the fundamental and the harmonics. As an example, ϕ_1, ϕ_2, ϕ_3, A_1, A_2, and A_3 are presented in Fig. 5 for time t=10.0 s, corresponding to the gas pressure p=416.8 mTorr.

The phase data show that higher harmonics have higher wave numbers, and they are not detectable until the wave has partially propagated through the dust cloud, as shown in Figs. 5(a)–5(c). The amplitude data show that the harmonics grow at faster rates than the fundamental, but never overcome the fundamental, Fig. 5(d). All amplitudes saturate near the bottom of the dust cloud at lower values of z.

In our phase-sensitive detection, we fit phase data, like those in Figs. 5(a)–5(c), to a line, yielding the wave number k_r. Likewise, we fit amplitude data, as in Fig. 5(d), to an exponential, yielding the growth rate $-k_i$, reported next.

D. Wave numbers and growth rates of harmonics

Results for the wave numbers k_r and the growth rates $-k_i$ are presented as functions of pressure in Figs. 6(a) and 6(b). For both the fundamental and the harmonics, we see distinctive values for k_r and $-k_i$ that vary little with pressure. The wave number did not vary noticeably at all, Fig. 6(a), while the growth rate had a slight trend to increase as p decreases, Fig. 6(b). In a previous report of a different experiment,[26] we noted this trend for the fundamental $-k_{i_1}$; here, we find the same trend for the harmonics $-k_{i_2}$ and $-k_{i_3}$ as well. Noise at high pressures in Figs. 6(a) and 6(b) is due to small wave amplitudes.

As one of our chief results, we find that the harmonic wave numbers and growth rates nearly double for the second harmonic, and triple for the third harmonic, as compared to the fundamental. This is demonstrated by calculating ratios of k_r in Fig. 6(c) and $-k_i$ in Fig. 6(d). Over a 5 mTorr range of pressure, the ratios for wave numbers are k_{r_2}/k_{r_1} in the range of 1.95–2.09 and k_{r_3}/k_{r_1} in the range of 2.92–3.12. Similarly, the ratios for growth rates are k_{i_2}/k_{i_1} in the range of 1.92–2.07 and k_{i_3}/k_{i_1} in the range of 2.82–3.04.

We are unable to definitively explain our phenomenological observation of a doubling and tripling of k_r and k_i for the second and third harmonics. One possible interpretation is in the context of three-wave mixing. Consider two ideal undamped waves, l and m, that interact to generate a third wave n. In the most general case, the two interacting waves l and m are completely independent wave fields that overlap spatially. The frequencies are expected to add as

$$f_n = f_l + f_m. \tag{1}$$

If these ideal waves propagate in the same direction and they are acoustic (i.e., dispersionless, $f \propto k$) one would expect that wave numbers will add as

$$k_n = k_l + k_m \tag{2}$$

for both the real and imaginary parts of the wave number. The generation of a second harmonic $2f$, for example, corresponds to $f_l = f_m = f$, where f is the fundamental frequency. For the generation of a second harmonic we would expect the wave number to double, i.e., to have a simple ratio $k_{r_2}/k_{r_1}=2$. Likewise, the wave number triples for the third harmonic, $k_{r_3}/k_{r_1}=3$.

The ideal wave mixing model described above generally assumes an infinite lossless nonlinear medium with a dispersionless wave incident at the fundamental frequency. Under these ideal circumstances, the frequencies and wave numbers will have precisely defined values. In our experiment, however, the sample region is finite in size (spanning only a few wavelengths), and it has strong dissipation that nearly balances a strong energy source. A dispersion relation developed in Ref. 26 for our experimental conditions predicts that

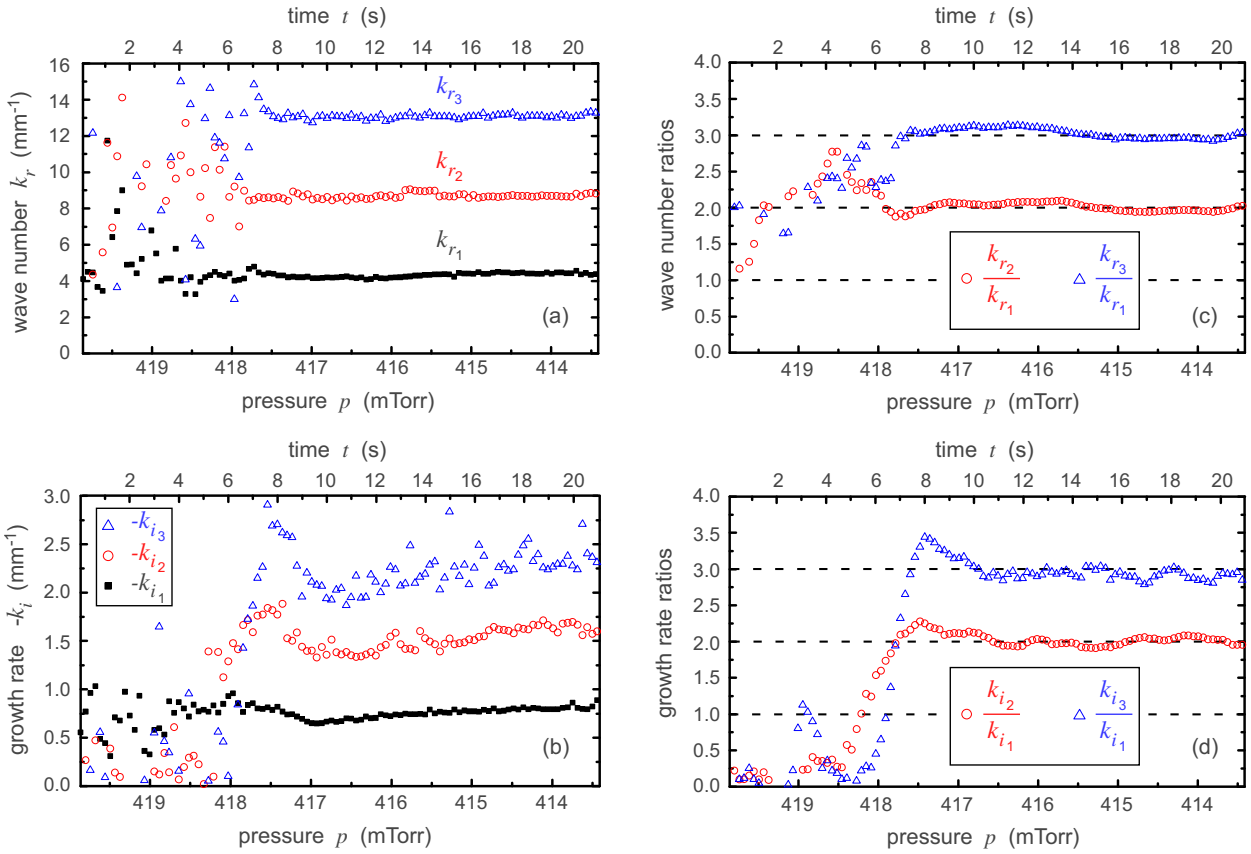

FIG. 6. (Color online) Measurements of (a) wave numbers k_r and (b) growth rates $-k_i$ as a function of gas pressure p. In (a), the real wave numbers for the fundamental mode k_{r_1}, second harmonic k_{r_2}, and third harmonic k_{r_3} do not vary with p. In (b), the growth rates of the same modes $-k_{i_1}$, $-k_{i_2}$, and $-k_{i_3}$ increase slightly as p decreases. (c) Wave number ratios k_{r_2}/k_{r_1} and k_{r_3}/k_{r_1} are close to two and three, respectively, when nonlinearity develops at lower pressures. (d) Growth rate ratios k_{i_2}/k_{i_1} and k_{i_3}/k_{i_1} are also two and three. In (a) and (b), scatter on the left is due to small wave amplitudes, which lead to noise in measurements of k_r and k_i. In (c) and (d), adjacent averaging is used to smooth data before calculating the ratios. Pressure and time scales are the same as in Fig. 4.

the wave has some dispersion in the frequency range f to $3f$, as shown in Fig. 7. We note that the dissipation and the finite system size could lead to a broadened bandwidth for the wave's frequencies and wave numbers. Thus, it is possible that the wave can propagate with a wave number and frequency which is slightly off the curve of the theoretical dispersion relation.

A doubling and tripling of $-k_i$ has been observed in experiments with a different kind of plasma wave. About 40 years ago, several experimenters measured the growth of unstable Langmuir waves using an interferometric method relying on a lock-in amplifier to provide phase-sensitive detection. Their waves grew as the result of an electron-beam driven instability. In three of the Langmuir-wave experiments, a doubling of $-k_i$ for the second harmonic and a tripling of $-k_i$ for the third harmonic were observed (Refs. 33–35). However, our inspection of the data from another similar experiment by Apel[36] reveals a departure from this integer multiplication of the growth rate, with measured $-k_i$ values less than integer multiples. Although there are some similarities between the results of these experiments and our results, the physical systems are not the same. For instance, in our experiment, the DDW is not in resonance with the ion-flow velocity, whereas the Langmuir wave's fundamental mode is in resonance with the electron-beam velocity. Additionally, the sources of nonlinearity may be different, and the time scales are much slower in our experiment.

In addition to the doubling and tripling of k_r and $-k_i$, one of our quantitative results was the amplitude of the harmonics. Suitable theories could be tested against the amplitudes we observed. It is unclear whether one can use the Manley–Rowe relations,[37] which are used most often to model an ideal nonlinear system without dissipation, driven by an external oscillator.

VI. SUMMARY

In a dusty plasma experiment, we study nonlinearity in a naturally occurring dust-density wave, which grows as it propagates. Our experimental design provides nearly planar wave fronts, which allows using phase-sensitive detection to measure the amplitude and phase for both the fundamental and the harmonic wave components. As a control parameter for nonlinearity, we adjust the gas pressure over a very small range near the critical pressure, where the ion-flow instability is in balance with gas damping.

As our first main result, we observe three conditions in the development of nonlinearity in the dust-density wave. The nonlinearity is indicated by the presence of harmonics with large amplitudes and is quantified by the THD. As gas

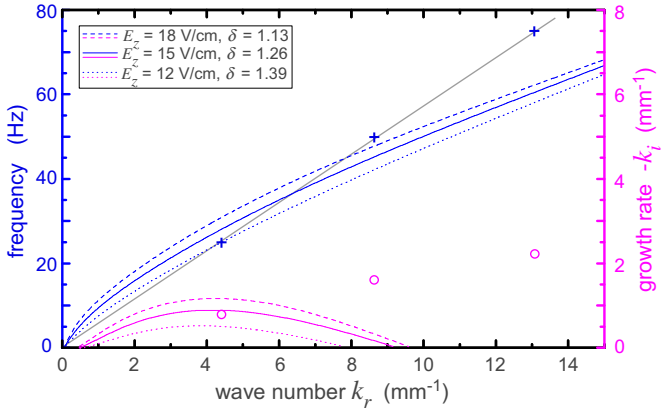

FIG. 7. (Color online) Three linear dispersion relations for the frequency (upper three curves) and spatial growth rate $-k_i$ (lower three curves) calculated from Eq. (6) of Ref. 26. The model's input parameters are explained in the Appendix of Ref. 26. The differences in the three curves reflect the uncertainty in our estimates of these input parameters. Also plotted are the experimental measurements of frequency (crosses) and $-k_i$ (circles) for the fundamental, second, and third harmonic modes. These frequency vs k_r measurements fall on a straight line (gray), as if they obeyed a purely acoustic dispersion relation. Both the experimental and model data are for 414 mTorr.

pressure p is reduced gradually, the three conditions observed are as follows: at high p the nonlinearity cannot be distinguished from noise; at intermediate p the nonlinearity increases exponentially over a limited range in p; and finally at lower p the nonlinearity no longer increases.

As our second main result, we find that the wave numbers and growth rates of the second and third harmonic modes are doubled and tripled, respectively, as compared to those of the fundamental. Such a doubling and tripling would be expected for an ideal wave with no dispersion or damping. Our observations for the doubling and tripling of the growth rate are similar to observations for Langmuir waves driven by a beam-plasma instability.

ACKNOWLEDGMENTS

We thank A. Ratner for helpful discussions. This work was supported by NASA (Contract Nos. NNX07AD22G and NNX10AR55G) and NSF (Contract No. 0903501).

[1]N. N. Rao, P. K. Shukla, and M. Y. Yu, Planet. Space Sci. **38**, 543 (1990).
[2]A. Barkan, R. L. Merlino, and N. D'Angelo, Phys. Plasmas **2**, 3563 (1995).
[3]M. Rosenberg, J. Vac. Sci. Technol. A **14**, 631 (1996).
[4]R. L. Merlino, Phys. Plasmas **16**, 124501 (2009).
[5]C. Thompson, A. Barkan, N. D'Angelo, and R. L. Merlino, Phys. Plasmas **4**, 2331 (1997).
[6]V. I. Molotkov, A. P. Nefedov, V. M. Torchinski, V. E. Fortov, and A. G. Khrapak, J. Exp. Theor. Phys. **89**, 477 (1999).
[7]V. E. Fortov, A. G. Khrapak, S. A. Khrapak, V. I. Molotkov, A. P. Nefedov, O. F. Petrov, and V. M. Torchinsky, Phys. Plasmas **7**, 1374 (2000).
[8]V. E. Fortov, A. D. Usachev, A. V. Zobnin, V. I. Molotkov, and O. F. Petrov, Phys. Plasmas **10**, 1199 (2003).
[9]S. Ratynskaia, M. Kretschmer, S. Khrapak, R. A. Quinn, M. H. Thoma, G. E. Morfill, A. Zobnin, A. Usachev, O. Petrov, and V. Fortov, IEEE Trans. Plasma Sci. **32**, 613 (2004).
[10]T. Trottenberg, D. Block, and A. Piel, Phys. Plasmas **13**, 042105 (2006).
[11]E. Thomas, Phys. Plasmas **13**, 042107 (2006).
[12]M. Schwabe, M. Rubin-Zuzic, S. Zhdanov, H. M. Thomas, and G. E. Morfill, Phys. Rev. Lett. **99**, 095002 (2007).
[13]I. Pilch, T. Reichstein, and A. Piel, Phys. Plasmas **16**, 123709 (2009).
[14]J. D. Williams and E. K. Snipes, IEEE Trans. Plasma Sci. **38**, 847 (2010).
[15]A. Piel, M. Klindworth, and O. Arp, Phys. Rev. Lett. **97**, 205009 (2006).
[16]A. Piel, O. Arp, M. Klindworth, and A. Melzer, Phys. Rev. E **77**, 026407 (2008).
[17]V. E. Fortov, O. F. Petrov, V. I. Molotkov, M. Y. Poustylnik, V. M. Torchinsky, V. N. Naumkin, and A. G. Khrapak, Phys. Rev. E **71**, 036413 (2005).
[18]P. Bandyopadhyay, G. Prasad, A. Sen, and P. K. Kaw, Phys. Rev. Lett. **101**, 065006 (2008).
[19]J. Heinrich, S.-H. Kim, and R. L. Merlino, Phys. Rev. Lett. **103**, 115002 (2009).
[20]C.-T. Liao, L.-W. Teng, C.-Y. Tsai, C.-W. Io, and I. Lin, Phys. Rev. Lett. **100**, 185004 (2008).
[21]M. Schwabe, S. K. Zhdanov, H. M. Thomas, A. V. Ivlev, M. Rubin-Zuzic, G. E. Morfill, V. I. Molotkov, A. M. Lipaev, V. E. Fortov, and T. Reiter, New J. Phys. **10**, 033037 (2008).
[22]J. Pramanik, B. M. Veeresha, G. Prasad, A. Sen, and P. K. Kaw, Phys. Lett. A **312**, 84 (2003).
[23]K. O. Menzel, O. Arp, and A. Piel, Phys. Rev. Lett. **104**, 235002 (2010).
[24]L.-W. Teng, M.-C. Chang, Y.-P. Tseng, and I. Lin, Phys. Rev. Lett. **103**, 245005 (2009).
[25]G. Joyce, M. Lampe, and G. Ganguli, Phys. Rev. Lett. **88**, 095006 (2002).
[26]T. M. Flanagan and J. Goree, Phys. Plasmas **17**, 123702 (2010).
[27]B. Liu, J. Goree, V. Nosenko, and L. Boufendi, Phys. Plasmas **10**, 9 (2003).
[28]R. K. Varma, P. K. Shukla, and V. Krishan, Phys. Rev. E **47**, 3612 (1993).
[29]K. N. Ostrikov, S. V. Vladimirov, M. Y. Yu, and G. E. Morfill, Phys. Rev. E **61**, 4315 (2000).
[30]M. R. Gupta, S. Sarkar, S. Ghosh, M. Debnath, and M. Khan, Phys. Rev. E **63**, 046406 (2001).
[31]J. B. Pieper, J. Goree, and R. A. Quinn, Phys. Rev. E **54**, 5636 (1996).
[32]J. H. Scofield, Am. J. Phys. **62**, 129 (1994).
[33]J. H. Malmberg and C. B. Wharton, Phys. Fluids **12**, 2600 (1969).
[34]K. Mizuno and S. Tanaka, Phys. Rev. Lett. **29**, 45 (1972).
[35]H. Mori, J. Phys. Soc. Jpn. **35**, 592 (1973).
[36]J. R. Apel, Phys. Rev. Lett. **19**, 744 (1967).
[37]J. M. Manley and H. E. Rowe, Proc. IRE **44**, 904 (1956).